Accepted for publication in
J. Geophys. Res.
November 2009

Climatology of aerosol optical depth in North-Central Oklahoma: 1992 - 2008

J. Michalsky, F. Denn, C. Flynn, G. Hodges, P. Kiedron, A. Koontz, J. Schlemmer and S. E. Schwartz

Abstract

Aerosol optical depth (AOD) has been measured at the Atmospheric Radiation Measurement (ARM) central facility near Lamont, Oklahoma, since the fall of 1992. Most of the data presented are from the multi-filter rotating shadowband radiometer, a narrow-band, interference-filter sunradiometer with five aerosol bands in the visible and near infrared, however, AOD measurements have been made simultaneously and routinely at the site by as many as three different types of instruments including two pointing sunradiometers. Scatterplots indicate high correlations and small biases consistent with earlier comparisons. The early part of this 16-year record had a disturbed stratosphere with residual Mt. Pinatubo aerosols, followed by the cleanest stratosphere in decades. As such, the last 13 years of the record reflect changes that have occurred predominantly in the troposphere. The field calibration technique is briefly described and compared to Langley calibrations from Mauna Loa Observatory. A modified cloud-screening technique is introduced that increases the number of daily-averaged AODs retrieved annually to about 250 days compared to 175 days when a more conservative method was employed in earlier studies. AODs are calculated when the air mass is less than six, i.e., when the sun's elevation is greater than 9.25º. The more inclusive cloud-screen and the use of most of the daylight hours yield a data set that can be used to more faithfully represent the true aerosol

climate for this site. The diurnal aerosol cycle is examined month-by-month to assess the effects of an aerosol climatology based on less frequent sampling such as that from satellites.

1. Introduction

Aerosol optical depth (AOD) measurements using sun radiometry yield the vertical column integral of the aerosol extinction coefficient measured from the surface to the top of the atmosphere. It is a robust measure of aerosol abundance, and, as such, this quantity is used to characterize geographical distribution, anthropogenic impact, radiative forcing of climate change, and aerosol's contribution to global dimming, i.e., the decrease in solar radiation reaching the earth's surface. Additionally, the wavelength dependence provides information on particle size. Determination of AOD by sunradiometry is especially robust compared to determination by down-looking radiance measurements from satellites; consequently, the surface-based determination of AOD by sunradiometry serves as ground truth for satellites, which, because of their global coverage, are better suited to determining the geographical distribution of aerosol loading and optical properties. Surface-based AOD measurements are suitable for evaluation of aerosol models; for identification of aerosols from specific events (e.g., the Central American fires (*Peppler et al.,* [2000])); and for monitoring temporal changes following events such as volcanic eruptions. Surface-based measurements offer diurnal coverage (during daylight hours), not otherwise available. McComiskey et al. [2008] showed for representative aerosol properties at SGP that an error in AOD at 550 of 0.01 results in an error in aerosol direct forcing of 0.6 and 1.3 W/m^2 at the top of the atmosphere and surface, respectively, for a solar-zenith-angle of 45°, and 0.3 and 0.5 W/m^2 for a 24-hr average at equinox.

Some multi-year aerosol optical depth (AOD) measurement records that were completed or were ongoing at the end of the last decade are summarized in Table 1. The largest AOD network is AERONET [*Holben et al.,* 2001], which uses a narrow field of view suntracking sunradiometer manufactured by CIMEL that measures transmittance of solar radiation in eight narrow wavelength bands. Networks that also use the CIMEL sunradiometer [*Holben et al.,* 1998], exclusively, and are affiliated with AERONET include PHOTONS (loaphotons.univ-lille1.fr), headquartered in France, and AEROCAN [*Freemantle et al*., 2005], headquartered in Canada. In addition, the first ten years of AOD data from the SURFRAD network, primarily a surface radiation budget measurement network, have recently been published [*Augustine et al.,* 2008].

The Atmospheric Radiation Measurement (ARM) program of the U.S. Department of Energy [*Stokes and Schwartz,* 1994] conducts AOD measurements at six locations; Alaska (2), the South Pacific (3) and the Southern Great Plains (SGP) of the United States. The SGP site, which covers an area in Oklahoma and Kansas that measures 300 × 400 kilometers, actually includes 21 AOD measurement sites. This array of sites has been used to study the temporal and spatial distribution of aerosols and to evaluate satellite aerosol products [*Alexandrov et al.,* 2002a; *Alexandrov et al.*, 2002b].

Farms that grow corn, wheat, and a few other crops, or that serve as pasture for cattle surround the central facility of the SGP site (36.605 ºN, l97.485 ºW). Central sources of pollution that could affect the site are to the east and northeast and, because of the prevailing southerly winds, rarely influence the site. All of the coal-fired power plants in Oklahoma are east of the SGP site http://www.sourcewatch.org/index.php?title=Oklahoma_and_coal - Existing_coal_p. Ponca City, an urban area of 25,000, contains an oil refinery, and there is a carbon black manufacturing

facility south of Ponca City, but all of these sources are well east of the site. The largest urban area is Oklahoma City some 130 km south of the site.

This paper provides an overview and analysis of AOD measurements for the central facility at which AOD measurements have been made continuously since 1992. It focuses on measurements made with the multi-filter rotating shadowband radiometer (MFRSR) that measures aerosol at five wavelengths between 415 and 870 nm using 10-nm wide (full width at half maximum) filters. Comparisons are made to the other long-term AOD measurements at the SGP central facility, which are sun-pointing sunradiometers, to further investigate the accuracy of the climatological record that is presented. A revised technique to screen for clouds is outlined and examined with several examples to assess the limits of applicability. Diurnal behavior as a function of month is examined. The availability of a long-term record of daily AOD measurements permits the investigation of the climatological representativeness of a single daily measurement or a few measurements each day, as might be obtained with a satellite or hand-held instrument, compared to more complete diurnal sampling.

2. Instruments, Calibrations, and Cloud-Screening

The MFRSR is fully described in *Harrison et al.* [1994], but a brief description follows: the MFRSR uses a horizontal diffuser that approximates a Lambertian receiver (one whose response decreases as the cosine of the angle of incidence); radiation that is transmitted through the diffuser reaches seven channels, including six filtered channels and an open channel that is used as a proxy measurement of broadband solar irradiance. A microprocessor-controlled procedure makes four measurements; one with the band at the nadir position; one just short of blocking the sun; one blocking the sun; and one just past the sun-blocked position. The two, near-sun stops

are used to calculate the excess diffuse radiation blocked by the band during the sun-blocked measurement. The direct is calculated by subtracting the corrected diffuse from the measurement with the band at the nadir position, whose difference is approximately the direct that would fall on a horizontal surface. After division by the cosine of the solar-zenith angle, corrections for the imperfect cosine response, based on pre-deployment laboratory characterizations, are applied. ARM also operates the normal incidence multi-filter radiometer (NIMFR) that uses the same receiver as the MFRSR, but it has a field of view with a full angular width of 5.7º and points at the sun continuously. This instrument was not deployed until the last half of the data record discussed in this paper.

The CIMEL sunradiometer points at the sun using a full field of view of 1.2º. There are significantly fewer data used in the CIMEL daily averages because the CIMEL only samples about every 15 minutes compared to MFRSR data that are sampled more frequently. For the first three years the MFRSR data were, either one-minute averages of samples taken once every 15 seconds, or single measurements made once every 15 seconds. The remaining 13 years of data are samples made once every 20 seconds. All NIMFR data are single samples made every 20 seconds.

Total optical depth $\tau(t,\lambda)$ is calculated for all sunradiometers using

$$\tau(t,\lambda) = \ln[(I_0(t,\lambda)/I(\lambda)]/m$$

where I_0 is the top-of-atmosphere solar irradiance for the passband at wavelength λ, I is the measured solar irradiance at the surface, and m is the pathlength through the atmosphere relative to the zenith direction, or air mass. The determination of I_0 is the calibration, which will be

discussed presently. The AOD is obtained in five wavelength channels by subtraction of the optical depth due to Rayleigh scattering and the ozone absorption optical depth.

The calibration technique used for all of the data in this paper, with the exception of those obtained with the CIMEL instrument, for which the AERONET protocol (*Holben et al.* [2001]) is followed, is briefly summarized here. The calibrations of the MFRSRs and NIMFR instruments used at the site are based on a field technique described in *Michalsky et al.* [2001]. The field technique is compared in this paper to traditional Langley calibrations performed on Mauna Loa, widely regarded as the premier site for these measurements.

Morning and afternoon data plots of the *ln(I)* versus *m* (a Langley plot) for air masses between 2 and 6 are screened for clear, stable periods as described in *Harrison and Michalsky* [1994]. All acceptable Langley-plot intercepts within a 60-day window, centered on the day for which a calibration is required, were used to estimate an instrument calibration for the five aerosol channels. The Langley plot intercepts, which are estimates of an instrument's response at the top of the atmosphere, are first normalized to unit Earth-Sun distance, and then a robust estimate for the calibration, employing the procedure described in *Michalsky et al.* [2001], is obtained for each day during the deployment of each MFRSR. Smoothing is applied to these daily Langley intercept estimates plus all of the individual Langley intercepts obtained in the first and last 30 days of the deployment. For the ARM site the uncertainties in the Langley plot intercepts is typically between 1 and 2% with the larger uncertainties in the summer because of fewer stable Langley plots. A 1% uncertainty in the intercept is approximately 0.01 AOD uncertainty at one air mass; the uncertainty decreases with inverse air mass. A deployment is usually terminated because of equipment failure, often the result of nearby lightning strikes. Eight different MFRSR

configurations were used in obtaining 16 years of data for the primary MFRSR site at the SGP central facility with continuous deployments as short as six months and as long as six years.

Comparisons of a non-ARM MFRSR calibrated by this field technique and also calibrated at Mauna Loa Observatory are shown in Figure 1 to demonstrate the veracity of the field technique even at a difficult site. The field calibration was performed at the CERES Ocean Validation Experiment (COVE, see cove.larc.nasa.gov) site on the Chesapeake Lighthouse. At the COVE site acceptable Langley plots are obtained infrequently, especially for the shorter wavelengths. The boxplots for Figure 1 are for the five filters used for aerosol measurements in the MFRSR indicated by the numerical suffix in nm, for example, the label 'mlo415' is the boxplot for Langley intercepts obtained at Mauna Loa Observatory (MLO) for the 415-nm filter. Four months of MLO Langley plots produced calibrations that are compared with three years of COVE Langley plot calibrations. In every case the spread in the COVE boxplots is larger. Most of this spread results from the less stable atmospheric conditions at COVE compared to the MLO site and the stability of the instrument caused by diffuser soiling or filter transmission losses, but some is caused by the annual variability of the Langley intercepts (see *Augustine et al.,* [2008]) that is generally attributed to ambient temperature effects on the Spectralon® diffuser. The median MLO intercepts are larger than the COVE intercepts, which is to be expected as the diffuser of the MFRSR soils and the interference filters degrade at the COVE site. The largest difference in medians is 4.3% for 415 nm, and the smallest is 0.3% for 673 nm. While the goal here was to validate the field calibration technique that is used to calibrate instruments at the SGP, Figure 1 demonstrates that the technique produces plausible calibrations compared to MLO calibrations, but this test should be repeated with Langley plots at MLO and SGP separated by months rather than the two-year separation represented here.

As the desired property from the measurements is aerosol optical depth, it is essential to screen against clouds. While such screening is trivial for thick clouds that totally obscure the sun, such screening is problematic for thin clouds whose contribution to optical depth might otherwise be ascribed to aerosols. In principal, approaches to cloud screening might rely on temporal variation of optical depth as the cloud is swept across the sun by the wind, or, alternatively, by the wavelength dependence of the optical depth, as cloud drops are sufficiently large that their optical depth exhibits little dependence on wavelength, in contrast to the typical significant wavelength dependence of aerosols.

Several approaches have previously been described for automating the cloud-screening process, all of which rely on time variations in AOD and not on the wavelength dependence. An example is the procedure for the AERONET network, which uses the CIMEL sun-tracking sunradiometers, described in *Smirnov et al.,* [2000]. The primary test for clouds in AERONET is to take three samples separated by 30 seconds and check their stability. *Alexandrov et al.* [2004] developed a procedure specifically for MFRSRs. It tests 5 minutes, or 15 points, of data at a time for stability by calculating a stability parameter $\varepsilon = 1 - \exp(\overline{\ln(\tau)})/\overline{\tau}$ that is independent of the magnitude of the AOD. Clearly, if τ (AOD) is fixed in time then ε is 0; a maximum value of ε that can be considered AOD variability is set by empirical determination. Another method [*Augustine et al.,* 2008] combines an earlier version of the method used in this paper with *Alexandrov et al.'s* [2004] method. Our unpublished attempts to automate cloud screening using the wavelength dependence have not yet proven successful, however, adding this capability in the future could potentially make cloud screening even more robust.

The approach employed here uses a two-step screening process making use of the individual data points. The cloud-screening technique used for this analysis looks at 10 consecutive minutes of data, that is, 30 measurements for the 20-second samples that constitute most of the data set. The first, coarser filter takes the difference between each adjacent measurement, generating 29 differences, and also calculates the maximum minus the minimum AOD in the window. If all 29 differences are less than 0.02 and if the range of measured AOD within the 10-minute window is less than 0.03, then the points pass the first filter. The 10-minute window is moved one time step (20 seconds) and the difference and range tests are repeated. Unique surviving points for the day are subjected to the second filter.

The second, more stringent, filter, which is also based on temporal variability, scales the allowed variability according to the magnitude of the AOD. A *LOWESS* (locally-weighted scatterplot smoother [*Cleveland,* 1979]), using two-thirds of the day's data at each point, is used to provide an estimate of the value of the AOD at each time step, however other methods that estimate the local magnitude of AOD are acceptable. Differences are taken between adjacent samples as above, and the range of AODs is again calculated for the 30-sample window. The absolute value of the largest of the 29 differences must be less than 0.1 of the estimated AOD at the midpoint of the 30-sample window, and the range must be less than 0.2 of the same estimate; for example, if the AOD was approximately 0.1, based on the LOWESS estimate, then this second test would allow differences between samples to be no greater than 0.01, and the range of AOD within the 30 samples cannot exceed 0.02. Higher values of estimated AOD relax these requirements accordingly. The 10-minute window is advanced one time step (20 seconds), and the tests are repeated. Each surviving datum passing both tests is considered a valid measurement of AOD and contributes to the daily average.

The second important property of the optical depth is its wavelength dependence, which is commonly reported as the Ångström exponent. The wavelength dependence of optical depth is assumed to follow $\tau = \beta\lambda^{-\alpha}$, where the wavelength λ is in μm, α is the Ångström exponent, and $\beta = \tau(1.0\mu m)$ is a normalized measure of the optical depth. The Ångström exponent is a qualitative measure of the size distribution of the particles contributing to the optical depth, ranging from near zero, for particles of diameter much greater than the wavelength, such as cloud drops, to about 2.5 for accumulation mode aerosol particles. Here the Ångström exponent is calculated using two optical depth measurements, specifically at 500 and 870 nm, as

$$\alpha = -\frac{\ln(\tau_{0.5}) - \ln(\tau_{0.87})}{\ln(0.5) - \ln(0.87)}.$$

The Ångström exponent time series can be visually examined for its temporal variation and also as a check on the cloud-screening algorithm.

Application of the cloud-screening algorithm is illustrated for three days to make a few key points. First, it should be noted that because we require 10 consecutive minutes of measurements it is inevitable that some clear-sky points are removed, as brief cloud passages would eliminate stretches of clear-sun views shorter than 10 minutes. Figure 2 is a plot of the optical depth for 30 September 2006 at the SGP central facility. There are 1832 total measurements of optical depth plotted with the sun above 9.25º of which 1480, shown in red, passed the screening criteria. Note that the AOD shown by the black points (which did not pass the screening criteria) is generally greater than that of the adjacent red points. Note also that there is a corresponding decrease in the Ångström exponent, indicating an increase in the size of the particles contributing to AOD; such an increase would be expected for clouds.

Figure 2 illustrates a difficulty in clearly separating aerosols and clouds. The blue circles in the time series shows a slight increase in AOD compared to the surrounding values and a slight reduction in Ångström exponent in the top and bottom panels, respectively. Because the variation is smooth in time it is unclear whether the points arise from an excursion to higher relative humidity, which would produce larger aerosols, or whether the points are measuring the effect of a very thin, uniform cloud. This may be an example of what *Koren et al.* [2007] call the twilight zone between clouds and aerosols. Since the cloud-screening technique relies on large deviations in the times series of optical depth, this sequence of points, showing modest variability, was identified as aerosol. Micropulse lidar images (not shown) and sonde measurements of dew point near the time of the blue-circled data suggest the possibility of very thin cirrus in the zenith. If these small deviations represent cirrus clouds, then the AOD is overestimated modestly by 0.01 to 0.02.

Figure 3 shows data for 13 October 2006; all 1737 points for which the solar elevation exceeded 9.25º, yielded AOD measurements that satisfied the acceptance criteria. Although AOD is quite variable on this scale with several excursions of nearly 0.02, similar to the magnitude of deviation that was seen on 30 September 2006 (blue circles in Figure 2) that suggests that thin clouds may have affected the data, all points survived the screening criteria and were identified as free of cloud interference. The identification of these points as cloud-free is, in this case, reinforced by the slow variation of the Ångström exponent over the course of the day. Furthermore, lidar images (not shown) indicate no hint of clouds of any type. Consequently, the optical depth changes are all attributed to aerosol variations, lending credibility to the cloud-screening procedure based on time variability only.

The ability of this screening technique to identify aerosols from 6 July 2006 where cirrus and even optically thick clouds were present is examined in Figure 4. On this day 403 out of 2291 possible samples were identified as clear. If the deviations and range in the second filter of the screening technique are reduced to half of their values, 377 points are still identified as clear with these stricter criteria (not shown). It should be mentioned here that the decisions regarding the chosen values for the point-to-point differences allowed and range within a 30-point window were based on testing several values and ultimately choosing parameters that represent a compromise between loss of data and cloud contamination. Note that despite the Ångström exponent not being used in the cloud screening technique, all of the points exhibited rather large values, 1.5 to 2, characteristic of cloud free aerosol measurements in the direction of the sun, in contrast to the excluded points which exhibited consistently lower values, indicative of clouds.

The modified cloud-screening method described above results in a substantial increase in the number of days for which an averaged AOD can be calculated. The previous method [*Michalsky et al.*, 2001] produced a daily average every second day, and with the current method there is a daily average two out of every three days. In the previous method a linear least squares fit was made to 30 consecutive minutes of data, and no single point could deviate by more than 0.01 AOD from this fit or the test for cloud-free conditions was considered a failure. There remain cases where AODs were screened as cloudy because there were fewer than 10 consecutive minutes of clear sky in the sun's direction or the aerosol varied rapidly because there were structured plumes of smoke, typically from field burning. There are also instances where very thin clouds may have been included as aerosol although the contribution to the total AOD is expected to be small (for example, the maximum increase in the AOD in the blue-circled region in the top of Figure 2 is only about 0.02).

Comparisons of Daily AOD Measurements

The C1 and E13 MFRSRs make simultaneously measurements near one another (C1 and E13 are site designations that happen to be co-located at the central facility) and within a few meters of the C1 NIMFR. The data compared are cloud-screened following the procedures described in the last section. The daily-averaged AOD comparisons of the C1 MFRSR to the C1 NIMFR for the years 2007 and 2006 are shown in Figures 5(a) and 5(b), respectively. The results are similar for the two years, with mean differences that are the same and slopes very close to, and insignificantly different from, unity. The effect of these small slope differences is strongly influenced by the sparse, high-valued AODs. Nonetheless, even for an AOD of 0.5, the difference in AOD caused by non-unity slopes is less than 0.01. The mean differences, which are wavelength independent, are more problematic. The cause of the differences is unclear: it may be that the angular responses, which are pre-measured in order to correct for the instrument's deviation from true cosine response, are changing as the diffuser degrades; it may be a subtle tilt in the receivers from ideal horizontal alignment; or some combination of the above, or it may just be the uncertainty and bias introduced by the field calibration of each instrument. In Figures 6(a) and 6(b) the E13 MFRSR detector head was different in 2007 than in 2006, and the mean differences and slopes do not match as well as in Figures 5(a) and 5(b). The 2007 detector head data are shown in Figure 6(a). What Figures 5 and 6 suggest is that MFRSRs produce subtle offsets in AODs that are less than or on the order of 0.015. We suspect that these are associated with small, field calibration differences or subtle angular response or tilt issues. It should be stated that the data shown in these two figures have the largest differences that we have seen in comparing daily averages for the ten years where we have two instruments measuring AOD. Note that these differences are consistent with the comparisons in *Mitchell and Forgan* [2003].

In Figures 7(a) and 7(b) the daily-averaged AODs for the three complete years of SGP central facility AERONET data between 1999 and 2001 are compared to the C1 and E13 MFRSR daily averages. AERONET uses the CIMEL sunradiometer that points at the sun with a 1.2° field of view, acquires data about every 15 minutes, and uses a different cloud-screening method than used by the MFRSR. Despite these differences data shown in the scatterplots of Figure 7 are close to the 1:1 line. The mean differences between CIMEL and MFRSRs are less than 0.01 and the slopes of the scatterplots are not statistically different from unity. The root-mean-square (RMS) differences are larger in Figure 7 than in Figures 5 and 6 because of the differences in sampling. Many more points are included in daily averages derived from the MFRSRs

4. Aerosol Optical Depth Climatology at the SGP site

Over 4000 daily-averaged AODs were retrieved for the sixteen-year period. Therefore, average daily values were retrieved, on average, two of every three days. There were ten gaps that exceeded two weeks, two that exceeded one month, and one that exceeded two months. The larger gaps were the result of equipment failures, but extended cloudy periods occasionally caused gaps that were a week or longer. On average there were two to three such gaps each year. The greater recovery of aerosol data resulted in higher daily-averaged AODs, especially in the summer months, compared to the previous results [*Michalsky et al.*, 2001].

The overall average AOD over the entire time period (27 November 1992 – 25 August 2008) was 0.16. Including and excluding the first three years that were affected by Mt. Pinatubo aerosols did not change the average. To put this average in context, it is lower than that reported for Greenbelt, Maryland, an urban U.S. east coast site, 0.23, and greater than that for Sevillita, New Mexico, a rural U.S. intermountain site, 0.08 [*Holben et al.*, 2001].

The more than 4000 points representing daily-averaged AODs at 500 and 870 nm are shown in Figures 8(a) and 8(b), respectively. The scale for Figure 8(a) is limited to AODs less than 0.4 to show more detail for the majority of the data; there are 131 values that exceed 0.4 at 500 nm. All AODs in Figure 8(b) were less than 0.4. The green solid line in Figure 8(a) and the red solid line in Figure 8(b) are robust, locally-weighted estimates (LOWESS) whose averaging window of three-months was chosen to help the eye follow the annual cycle. As the LOWESS estimates at the endpoints of the record are disproportionately influenced by the border values, these estimates may not be true representations of terminal values. This is especially pertinent to the summer estimate in 2008 for which the day-to-day variability is much higher than at other times of the year. The 1992-1993, winter estimate may be nearly accurate because day-to-day values of AOD in the winter are more stable. As has been seen in many other studies [*Holben et al.*, 2001; *Michalsky et al.,* 2001], the aerosol loading peaks in the summer months and is a minimum in the winter. The summertime maxima vary considerably year-to-year whereas the winter minima are more stable. In the early years of this record the contribution to AOD from residual stratospheric aerosol resulting from the eruption of Mt. Pinatubo in June 1991 was substantial; the persistence of these aerosols can be seen in Figures 8(a) and, especially, 8(b) through, at least, the 1994-1995 winter. Such an influence of the Pinatubo aerosol on winter AOD has been noted previously [*Holben et al.*, 2001; *Michalsky et al.,* 2001]. A visual inspection of Figures 8(a) and 8(b) suggests little indication of a temporal trend over the time series. One feature to note is the upward tendency of the winter minima at both wavelengths over the last several years; this is clear in both the LOWESS fit and the individual data points. A few more years of data are needed to determine whether this indicates a clear trend in background aerosol loading, which will be most evident in the winter minima. A more extensive examination of trends follows.

The annual cycle of AOD is examined in Figure 9, which is a composite plot of all daily values for the entire record subsequent to October 1995 (excludes Pinatubo aerosols) as a function of day of year. The peak extinction occurs in the middle of summer and the minimum is at the beginning of winter, therefore, the annual cycle in aerosol loading is asymmetric. The day-to-day variations are pronounced during all times of the year, but the highest absolute variability occurs during the summer. For any day of the year AOD can exceed the LOWESS fit by more than 100%, therefore, uncertainties introduced by using climatological values of AOD in radiative transfer models can be substantial.

The Ångström exponent (α), defined earlier, for the 16-year record is plotted in Figure 10. For typical continental sites α is in the range 1.0 - 1.5, e.g., *Holben et al.*, [2001]. Clearly, this was the case for most of the record under examination; the exception was the period before 1995, for which the aerosol column was strongly influenced by the stratospheric aerosol from the Pinatubo eruption. The LOWESS fit with a six-month window (in red) chosen to approximate the seasonal values indicates higher values of α in summer and lower values in winter. As a larger Ångström coefficient is indicative of an aerosol consisting of smaller particles, this is consistent with the greater contribution to aerosol optical depth by small particles produced by photochemical reactions during the summer. The inter-annual trend indicated in Figure 10 by the LOWESS fit with a 12-month window (in blue) shows a clear increase in α associated with the depletion of Mt. Pinatubo aerosols from the stratosphere. The Ångström exponent exhibited a weak maximum around 1997-1998, followed by a slow decline until the present, the reasons for which are not known. The only exception to this trend is the 2002-2003 period, which saw an increase in aerosol optical depth and α possibly due to transported aerosols from the widespread fires in the western states during that period [*Augustine et al.,* 2008]. A composite plot of the 13 years of

Ångström coefficient data after October 1995 (excludes Mt. Pinatubo aerosols) is given in Figure 11. There is interesting structure in this plot: first, the highest values occur in late August indicating the smallest particles of the year; the lowest Ångström coefficients, and therefore, largest particles are found in late December and late April. Winter minima in particle size are typical of continental sites, but the second minimum in April may be associated with the transport of Asian aerosols to the U.S., which was also found for the western U.S. SURFRAD sites in Augustine et al. (2008). Finally, there are secondary minima around mid-July and early October that approximately coincides with harvesting and fall planting activity, respectively; these farming activities increase the airborne dust, which are, of course, large particles.

The annual-averaged data for the complete years in the record are summarized using boxplots in Figure 12. The boxplots demonstrate that the annual medians vary considerably, with the lowest and highest median differing by as much as 50% (e.g., compare 1998 and 1999). The differences in the inter-quartile ranges are large, as well. The means are plotted as large red dots above the horizontally-drawn medians. The red, dashed line is a fit to the annual means, excluding the first three years when stratospheric aerosols from the Mt. Pinaubo eruption could still be detected. The slope is 0.0097 optical depths per decade with a standard deviation of 0.0136; this is obviously statistically insignificant. Plotting the data in this way confirms the preliminary conclusion reached earlier concerning the absence of any significant trend in AOD at this location over the period of record. This contrasts with the recent paper by Mischenko et al. (2007), where it is reported that the aerosol optical depth (at least over the oceans) has decreased by 0.03. However, this is not an apples-to-apples comparison since we are comparing a single site in the center of North America with an integrated measurement over the oceans.

To assess diurnal variability, we examined five complete years of data 2003-2007 for each calendar month; this time period was selected because the same instrument was used throughout, thereby obviating concern about the bias arising from instrument changes. Every 20-second sample that survived the screening procedure is included. Data are shown only for times when the sun was at least 9.25º above the horizon for the shortest day in the month so as not to bias the end points. The data that survived the cloud-screening process for each day were divided by the average of all surviving points. These normalized values were binned for the five-year period for the hour of the day and month of the year. The beginning and end hours of the day for each month were generally not complete hours because of the restriction of the solar elevation to 9.25º and higher. The data were then multiplied by the average of the daily averages for five years of the same month. Boxplots of these data in Figure 13 illustrate daily trends for each month of the year. The scale is the same for each subplot to facilitate comparisons. For all monthly frames the medians of each hour are nearly the same and the inter-quartile ranges are similar, suggesting little or no diurnal trend. The smallest variations occur in the middle of the day as seen by the length of the whiskers, and the variations are progressively larger for hours earlier and later than this. The outliers capture rare events where large AOD values persist a short time, note, for example, the hour spanning 1600-1700 in the January data. During February the medians are higher than in January, the inter-quartile ranges are larger but again overlapping, and the whiskers, which indicate scatter, are similar except for the end boxes. In March and April the medians are incrementally higher than February and March, respectively, with overlapping, and somewhat larger, inter-quartile ranges, and no pattern in the extent of the whiskers from one hour to the next. The medians continue to rise from May to June and to July, and there is a tendency in these months for the afternoon AOD medians to be slightly higher than the morning, but the

differences are not statistically significant. August is slightly lower and the morning-afternoon difference is not apparent. In September medians drop, and then a large change in terms of lower AODs occurs for October, November, and December with progressively lower scatter in these months; note the size of the inter-quartile range. These data thus indicate, at least statistically, that little bias in long-term trends would arise from sampling the AOD at a given time of day, as would be the situation for measurement by sun-synchronous satellite, instead of this more complete sampling for the daily average.

The daily diurnal trend based on these five years, Figure 14, shows that the median AOD values differ by less than 0.005 over the course of the day. The large number of AOD measurements included in each boxplot is noted below each box. The lack of diurnal variation in AOD is surprising in view of the fact that the aerosol scattering coefficient increases strongly with relative humidity and the expectation of higher relative humidity in the boundary layer in the early morning and late afternoon. There is a noticeable change in the variability over the course of the day, with boxes and whiskers that are smallest at midday and progressively larger with increasing departure in time from midday, both earlier and later. Clearly, the variability is not correlated with the number of AOD measurements within the hour.

Discussion and Summary

The approach taken to establish the aerosol climatology was to weight every measurement of AOD on a single day equally in computing the daily-averaged AOD. On a day where, for example, the morning has many fewer measurements than the afternoon, this approach yields an average AOD that is more heavily influenced by the afternoon. Such a weighting might be appropriate in consideration of direct radiative forcing, where the aerosol forcing is effective

only in cloud-free sky. In computing long-term (monthly, annual) averages the procedure was to weight each day's AOD equally. An alternative might have been to weight the values by the number of measurements on a given day; however, a cloud-free day with low AOD would exert more influence on the derived climatology than that of partly cloudy days and skew the results producing a non-representative aerosol climatology.

The goal of this paper was to present a new and more representative aerosol climatology for a single site based on as complete a record for that site as was practical. The same type of instrument (MFRSR) was used for the entire record. Most of the measurements were taken every 20 seconds, but a few years at the beginning had 15-second samples and one-minute averages of 15-second samples. The field calibration technique that is used, so that the instrument does not have to be removed and interrupt the record, was described and partially validated by comparing field calibrations with Mauna Loa calibrations; however, the time between calibrations compromised the comparison. Acceptable comparisons were also made with side-by-side pointing instruments calibrated either using this field technique or using calibrations transferred from instruments calibrated on Mauna Loa.

A modified method for cloud-screening was described and illustrated. This method results in a substantial increase in the number of days for which an averaged AOD can be calculated (a previous method produced a daily average every second day and with this method there is a daily average two out of every three days). There are cases where AODs were screened as cloudy because there were fewer than 10 consecutive minutes of clear sky or the aerosol varied rapidly because there were structured plumes of smoke from field burning, for example. There are also some instances where very thin clouds have likely been included as aerosol although the absolute contribution to the total extinction is expected to be small.

The major features of AOD over the entire time period were a pattern of large AODs in the summer, and smaller AODs in the winter. A second major feature is the systematic variation of particle size over the annual cycle, with a minimum size in summer and maximum size in winter. A third feature was the influence of the stratospheric aerosol arising from Mt. Pinatubo following its eruption in June, 1991, that resulted in higher values of AOD and lower values of Ångström exponent through the winter of 1994-1995. The entire data set demonstrates the large day-to-day variability of aerosol optical depth, even at a mid-continental location that is quite far removed from major urban source regions, and the resultant limitations of using climatological values of AOD as input to radiative transfer models or for evaluation of chemistry and transport models. Aerosol optical depth was found to exhibit little systematic variation over the course of the daylight hours. As a final note, there is a slight increase in AOD that is not statistically significant, therefore, there is no clear, long-term trend in the nearly 16-year record of AOD suggesting that the diffuse horizontal irradiance brightening found by et *Long al.* [2009] at this site is not primarily caused by aerosols.

Acknowledgments

This research was supported in part by the Office of Biological and Environmental Research of the U.S. Department of Energy as part of the Atmospheric Radiation Measurement Program. The data from the COVE site are funded by the NASA Earth Observing System project.

References

Alexandrov, M., A. A. Lacis, B. E. Carlson, and B. Cairns, Derivation of 2D fields of aerosol and trace gases parameters by integrated analysis of multi-instrument MFRSR dataset from

DOE ARM Program CART site, in *Remote Sensing of Clouds and the Atmosphere VI*, K. Schafer, O. Lado-Bordowsky, A. Comeron, M. R. Carleer, J. S. Fender, Editors, Proc. SPIE Vol. 4539, 277-288, 2002a.

Alexandrov, M., B. Cairns, A.A. Lacis, and B.E. Carlson, Integrated study of MFRSR-derived parameters of atmospheric aerosols and trace gases over the ARM CART site: Comparison with satellite and other ground-based measurements, in Proceedings of the Twelfth ARM Science Team Meeting, ed. by D. Carrothers, U.S. Department of Energy, Richland, WA, 2002b.

Alexandrov, M. D., A. Marshak, B. Cairns, A. A. Lacis, and B. E. Carlson, Automated cloud screening algorithm for MFRSR data, Geophys. Res. Lett., 31, L04118, doi:10.1029/2003GL019105, 2004.

Augustine, J. A., G. B. Hodges, E. G. Dutton, J. J. Michalsky, and C. R. Cornwall, An aerosol optical depth climatology for NOAA's national surface radiation budget network (SURFRAD), *J. Geophys. Res., 113*, D11204, doi:10.1029/2007JD009504, 2008.

Cleveland, W.S., Robust locally weighted regression and smoothing scatterplots, *J. Am. Stat. Assoc.,* 74, pp. 829-836, 1979

Freemantle, J. N. O'Neill, A. Royer, B. McArthur, I. Abboud, AEROCAN: the Canadian Sunphotometer Network, Remote Sensing of Atmospheric Aerosols, 10.1109/AERSOL.2005.1494146, 2005.

Harrison, Lee, Joseph Michalsky, and Jerry Berndt, Automated multifilter rotating shadow-band radiometer: An instrument for optical depth and radiation measurements, *Appl. Opt.,* 33, 5118-5125, 1994.

Harrison, L. and J. Michalsky, Objective algorithms for the retrieval of optical depths from ground-based measurements, *Appl. Opt., 33,* 5126-5132, 1994.

Holben, B. N., et al., AERONET--A federated instrument network and data archive for aerosol characterization, *Remote Sens. Environ., 66*, 1-16, 1998.

Holben, B. N. et al. An emerging ground-based aerosol climatology: Aerosol optical depth from AERONET, *J. Geophys. Res., 106*, 12,067-12,097, 2001.

Koren, I., L. A. Remer, Y. J. Kaufman, Y. Rudich, and J. V. Martins, On the twilight zone between clouds and aerosols, *Geophys. Res. Lett.*, 34, L08805, doi:10.1029/2007GL029253, 2007.

Long, C. N., E. G. Dutton, J. A. Augustine, W. Wiscombe, M. Wild, S. A. McFarlane, and C. J. Flynn, Significant decadal brightening of downwelling shortwave in the continental United States, J. Geophys. Res., doi:10.1029/2008JD011263, 2009, in press.

McComiskey A., S.E. Schwartz, B. Schmid, H. Guan, E.R. Lewis, P. Ricchiazzi, and J.A. Ogren, Direct aerosol forcing: Calculation from observables and sensitivities to inputs, *J. Geophys. Res.*, 113, doi:10.1029/2007JD009170, 2008.

Michalsky, J., J. Schlemmer, W. Berkheiser III, J. Berndt, L. Harrison, N. Laulainen, N. Larson, and J. Barnard, Multi-Year Measurements of Aerosol Optical Depth in the Atmospheric Radiation Measurement and Quantitative Links Programs, *J. Geophys. Res. 106,* 12099-12107, 2001.

Mishchenko, Michael I., Igor V. Geogdzhayev, William B. Rossow, Brian Cairns, Barbara E. Carlson, Andrew A. Lacis, Li Liu, and Larry D. Travis, Long-Term Satellite Record Reveals Likely Recent Aerosol Trend**,** *Science* **315**, 1543 [DOI: 10.1126/science.1136709].

Mitchell, R. M. and B. W. Forgan, Aerosol Measurement in the Australian Outback:

Intercomparison of Sun Photometers, *J. Atmos. Ocean. Tech., 20*, 54-66, 2003.

Peppler, R.A., et al., ARM Southern Great Plains site observations of the smoke pall associated with the 1998 Central American fires, *Bull. Amer. Meteor. Soc.,* 81, 2563-2591, 2000.

Smirnov, A., B. N. Holben, T. F. Eck, O. Dubovik, and I. Slutsker, Cloud screening and quality control algorithms for the AERONET database, *Remote Sens. Environ., 73,* 337-349, 2000.

Stokes, G. M. and S.E. Schwartz, The Atmospheric Radiation Measurement (ARM) program: Programmatic background and design of the cloud and radiation test bed, *Bull. Amer. Meteor. Soc.,* 75, 1201-1221, 1994.

Table 1. Current Operational AOD Networks

Reference	Coverage	Tenure	Notes
BOM/CSIRO [*Mitchell and Forgan*, 2003]	Australia (17)	1984 – now	Middleton SP01, 02, CIMEL CE318
AERONET, [*Holben et al.,* 2001] (aeronet.gsfc.nasa.gov)	Global (110 sites > than 2 years of data)	1993 - now	CIMEL CE318
SKYNET (atmos.cr.chiba-u.ac.jp)	East Asia (11)	1996 – now	Prede POM01, 02
USDA [*Bigelow et al.,* 1998] (uvb.nrel.colostate.edu)	USA (37)	1995 – now	YES MFR7
SURFRAD [*Augustine et al.,* 2008] (www.srrb.noaa.gov)	USA (7)	1997 – now	YES MFR7
ARM (www.arm.gov)	USA, S. Pacific Ocean	1992 – now	YES MFR7, CIMEL CE318

Figure Captions

Figure 1. Boxplots of Langley intercepts taken at Mauna Loa Observatory and Chesapeake Bay Lighthouse – each boxplot has been normalized to the MLO median at every wavelength. COVE medians are lower, and the spread in Langley intercepts is larger.

Figure 2. Time series of AOD at 500 nm and the Ångström exponent (C1 MFRSR) are shown

for 30 September 2006 in local standard time, which is UTC minus six hours. Each point represents a single 20-second sample; data that survived the cloud screening tests are shown in red; points in black were considered cloud contaminated. Note corresponding decrease in Ångström exponent indicative of larger particles. Data in the blue circles, showing slight increase in AOD and size, are not excluded by cloud screening tests; these data may indicate a brief period of enhanced relative humidity (almost cloud) or possibly a very thin uniform cloud that is not identified by the cloud-screening algorithm.

Figure 3. Cloud-screened time series of AOD and Ångström exponent for 13 October 13 2006 in local standard time. On this day all points for which the sun was above elevation 9.25 ˚ were identified as aerosol. Despite considerable temporal variability in AOD on both shorter (minutes) and longer (hours) time scales, the Ångström exponent plot suggests no contribution from large particles (clouds).

Figure 4. Time series of AOD and Ångström exponent for 6 July 2006 in local standard time. Data points that passed cloud screening are in red. Figure illustrates the ability of the cloud-screening technique to select clear-sky points on a day dominated by thin cirrus and optically thick clouds.

Figure 5. (a) Scatterplot of 500-nm, daily-averaged AOD for 2007 obtained from the C1 MFRSR versus the C1 NIMFR. The black diagonal line is perfect correlation. (b) Same scatterplot for 2006. Note that the mean differences and root-mean-squared differences are identical to three significant figures.

Figure 6. (a) Scatterplot of 500-nm, daily-averaged AOD for 2007 obtained from the E13 MFRSR versus the C1 NIMFR. The black diagonal line is perfect correlation. (b) Same scatterplot for 2006. Note that the root-mean-squared differences are similar, but the mean difference changed sign; there was a MFRSR head change early in 2007.

Figure 7. (a) Scatterplot of the daily-averaged AOD at 500 nm measured by the AERONET CIMEL sunradiometer versus the C1 MFRSR for three years. (b) Scatterplot of the daily-averaged AOD at 500 nm measured by the AERONET CIMEL sunradiometer versus the E13 MFRSR for three years. Mean differences between MFRSRs are small, but measurable. Note the larger root-mean-squared differences compared to Figures 5 and 6.

Figure 8. (a) Black points are the daily-averaged AOD at 500 nm at the Department of Energy Southern Great Plains Central Facility in north central Oklahoma, from November 1992 to August 2008. Over 4000 points are shown; not shown are 131 points for which AOD exceeded 0.40. Green line is LOWESS fit showing seasonal variation (three-month averaging window); omitted high-AOD points were included in calculating the LOWESS estimate. (b) Black points are over 4000 daily averages of AOD at 870 nm. Red line is the LOWESS estimate with a three-month window that yields the approximate seasonal behavior of the AOD. All AODs at 870 nm were smaller than 0.40.

Figure 9. Thirteen years of data overlain on one-year to examine the annual variability. The LOWESS estimate in red uses a two-month window. The aerosol peaks in mid-summer and is a minimum at the beginning of winter.

Figure 10. The Ångström coefficient for the daily AOD averages in Figure 8. The LOWESS estimate, which uses a six-month window is in red, shows the seasonal variability and the inter-annual (12-month window) smoother in blue shows the longer-term changes. The largest particles occur in the winter months (smallest exponent) with the smallest particles in the summer (larger exponents).

Figure 11. Thirteen years of data overlain on one-year to examine the annual variability in the Ångström coefficient. The LOWESS estimate in red uses a two-month window. The aerosol size is a minimum near the end of August and is the largest at the beginning of winter and mid-April when Asian aerosol often adds to the aerosol column. The dips before day 200 and day 300 may be associated with increased farming activity that increase the airborne dust around the site.

Figure 12. Boxplots of each complete year's daily-averaged AOD at 500 nm. The dark horizontal line in each boxplot is the median daily-averaged AOD for the year; the top and bottom of the rectangular box spans the middle 50% of the data. The whiskers are drawn a distance of 1.5 times the length of the box above the top or bottom of the box or to the last point with an AOD nearer than this. Points beyond this range are plotted individually, however, points beyond 0.45 AOD are not shown. The mean values for the year are plotted as red dots, and these lie above the median bars for every year. The dashed red line denotes trend line over the period 1996-2007 inclusive; the first three years, which were influenced by stratospheric aerosol from the Pinatubo eruption, are excluded.

Figure 13. Boxplots of cloud-screened 20-second samples of AOD at 500 nm aggregated by time of day and month for 2003-2007, inclusive; local noon occurs between 12:00 and 13:00 since the longitude is about 97.5 °W. End points may not be complete hours.

Figure 14. Boxplots of cloud-screened 20-second samples of AOD at 500 nm aggregated by time of day for entire year for period 2003-2007, inclusive; local noon occurs between 12:00 and 13:00 since the longitude is approximately 97.5 °W. The number of 20-second samples in each boxplot is given below the box.

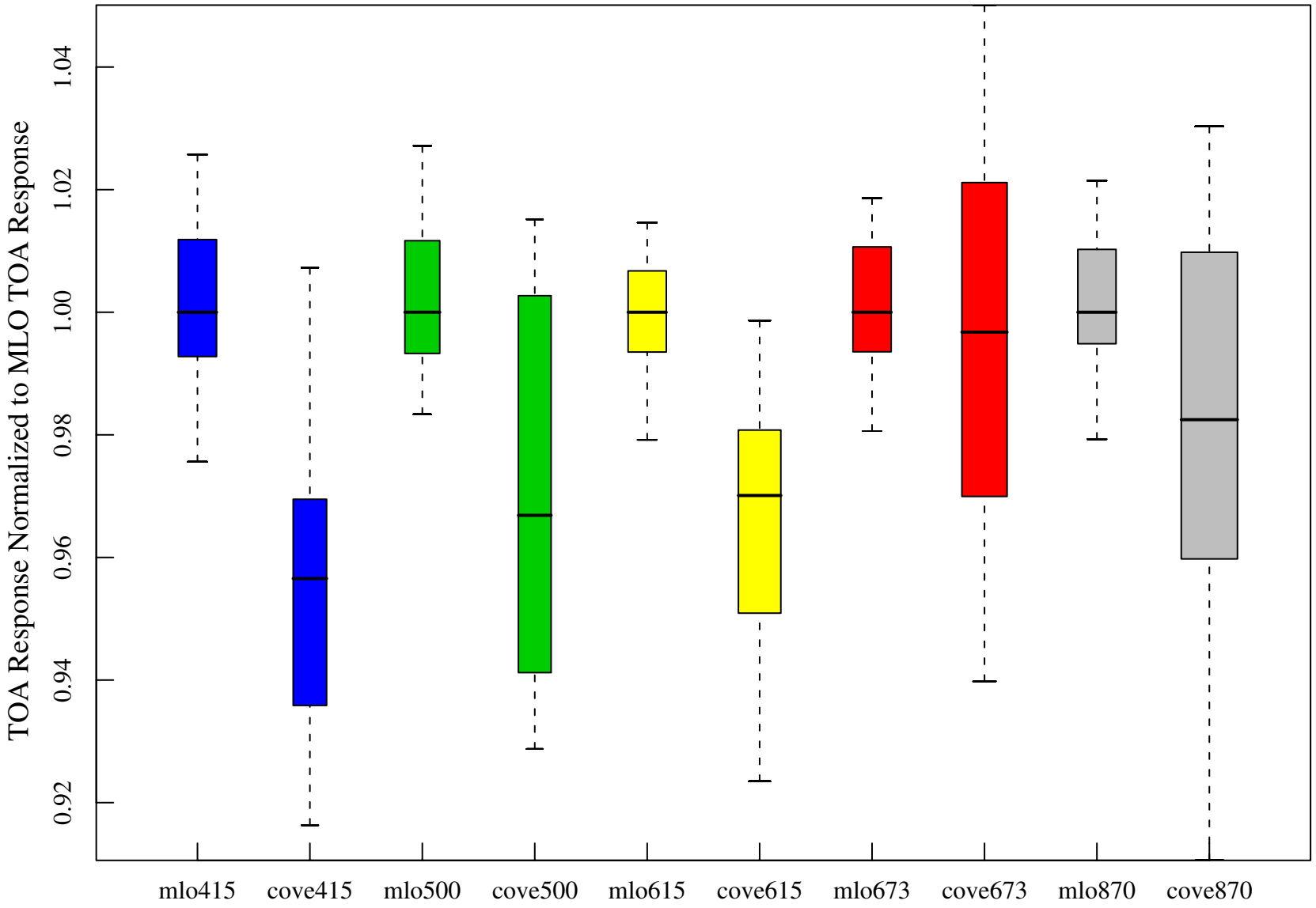
TOA Response Normalized to MLO TOA Response
0.92
0.94
0.96
0.98
1.00
1.02
1.04
mlo415
cove415
mlo500
cove500
mlo615
cove615
mlo673
cove673
mlo870
cove870

Figure 1

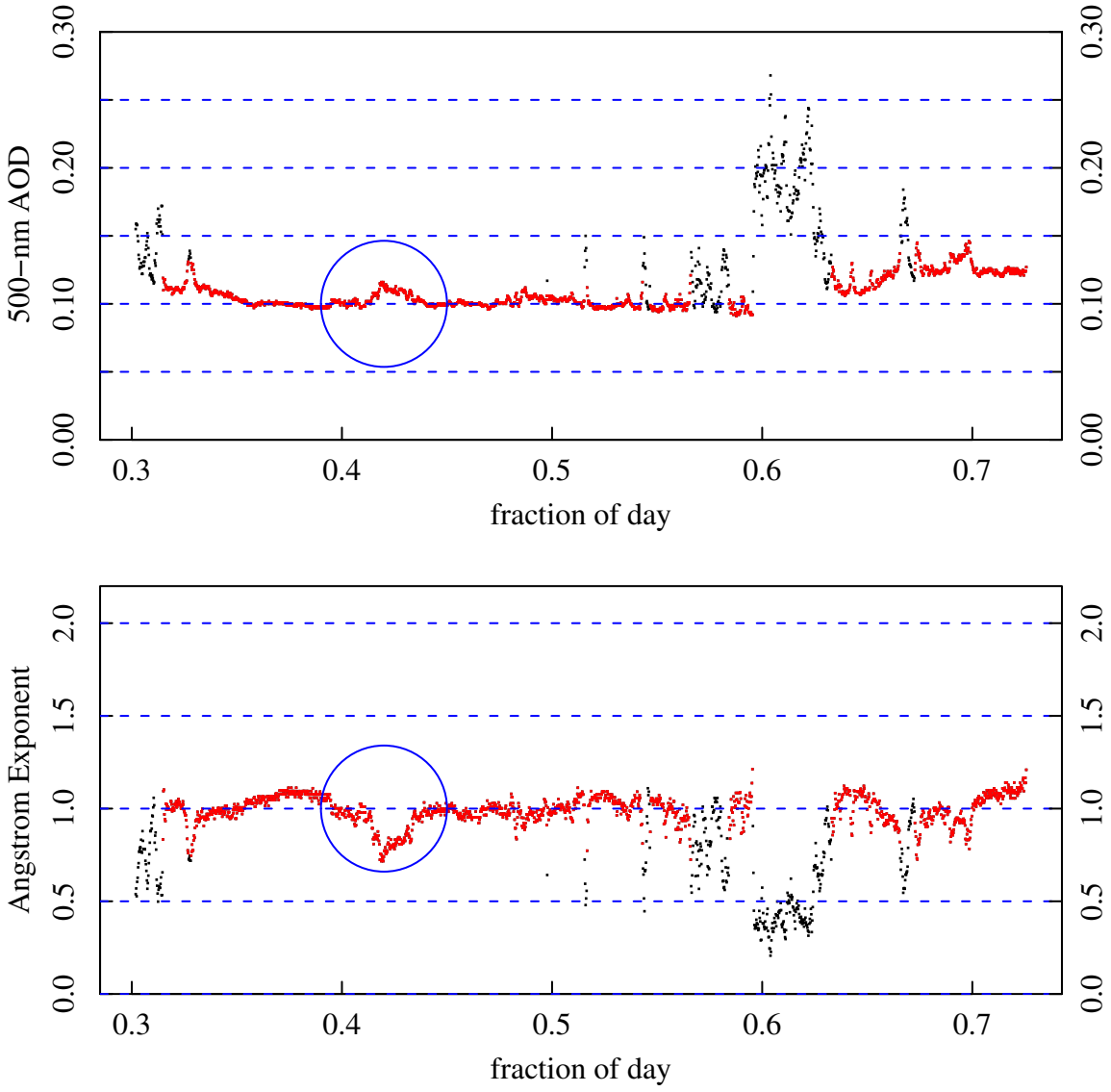
500−nm AOD
0.00
0.10
0.20
0.30
0.3
0.4
0.5
0.6
0.7
fraction of day
Angstrom Exponent
0.0
0.5
1.0
1.5
2.0
0.3
0.4
0.5
0.6
0.7
fraction of day

Figure 2

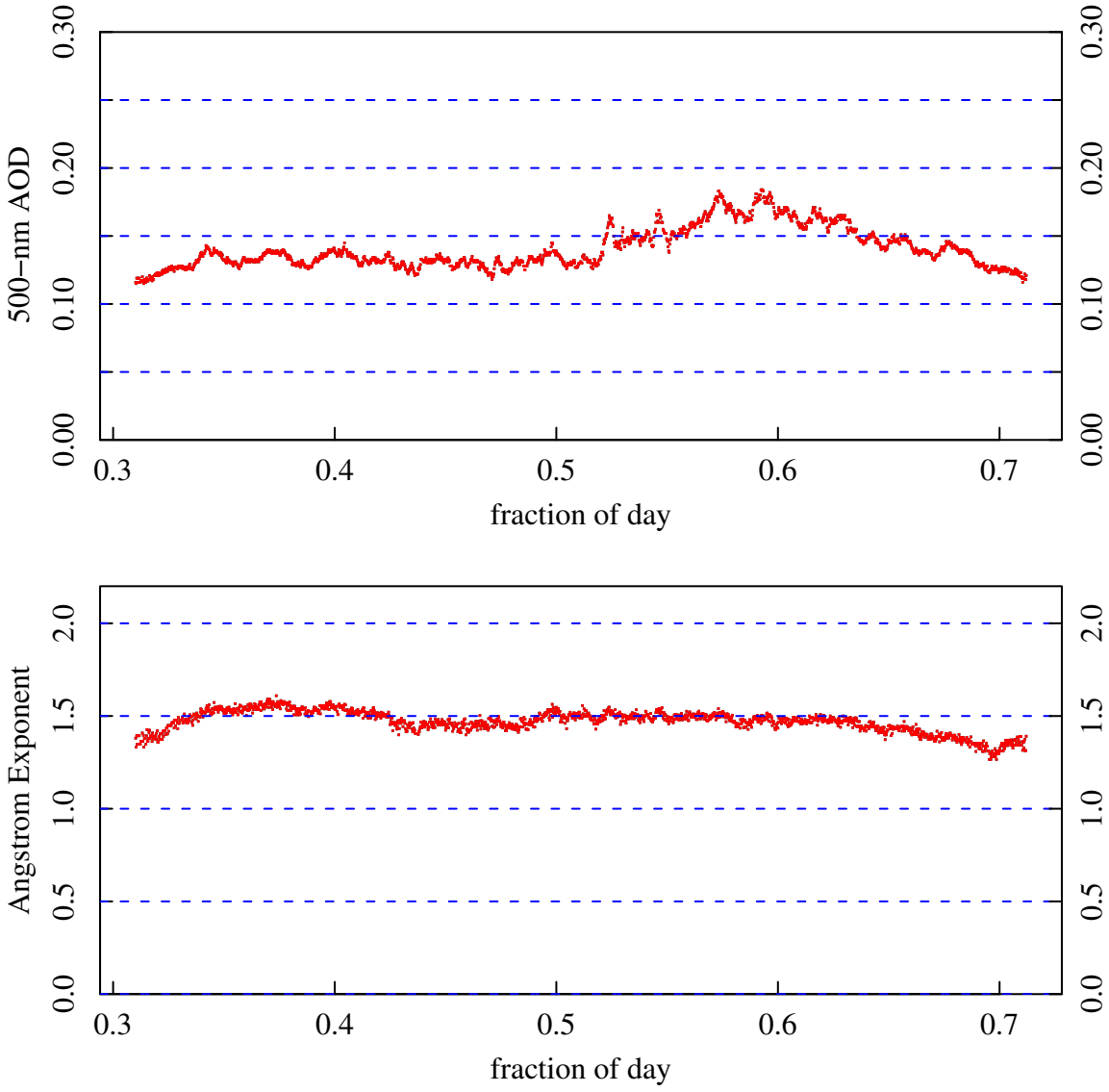
500−nm AOD
0.00
0.10
0.20
0.30
0.3
0.4
0.5
0.6
0.7
fraction of day
Angstrom Exponent
0.0
0.5
1.0
1.5
2.0
0.3
0.4
0.5
0.6
0.7
fraction of day

Figure 3

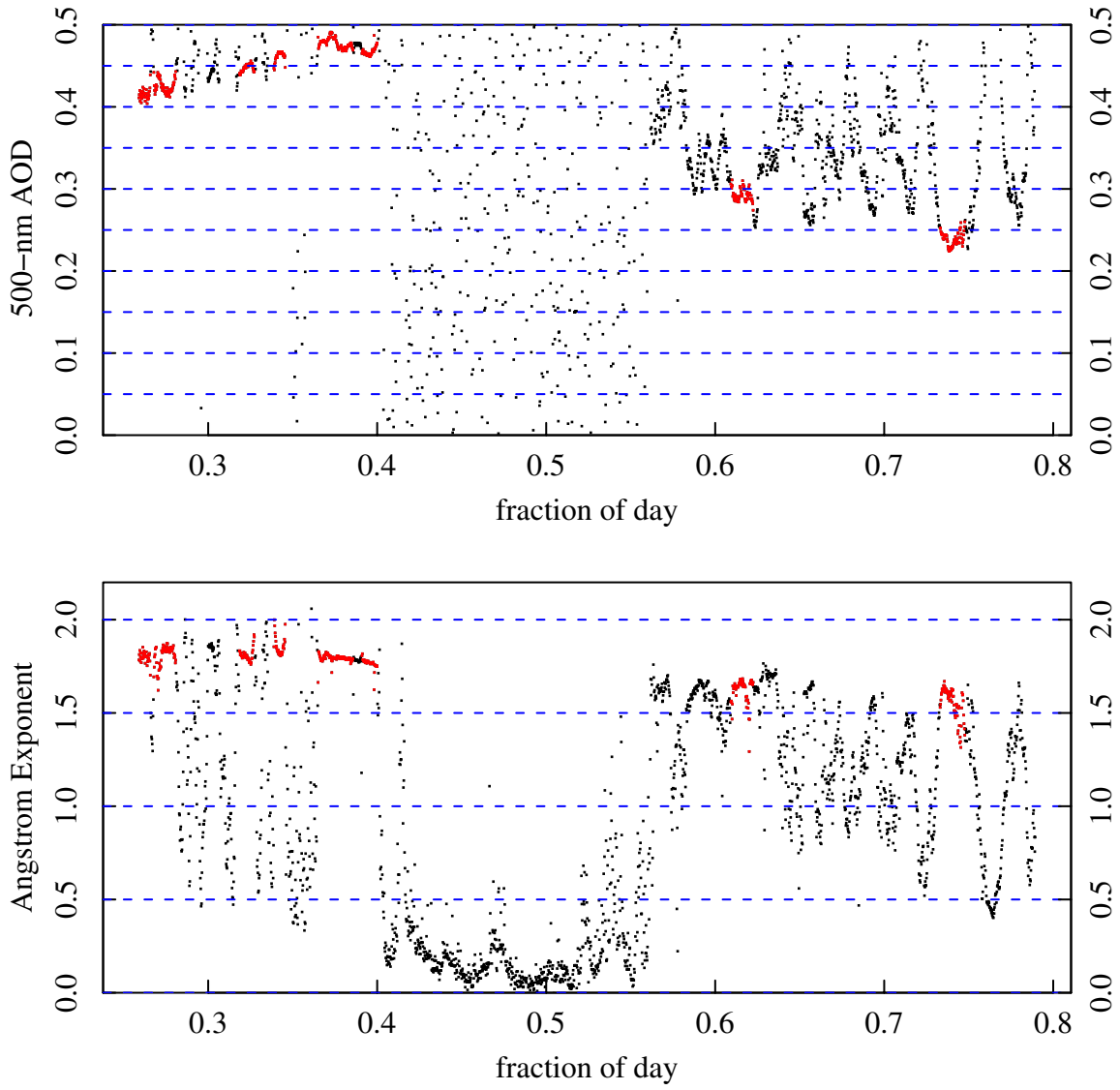
500−nm AOD
0.0
0.1
0.2
0.3
0.4
0.5
0.3
0.4
0.5
0.6
0.7
0.8
fraction of day
Angstrom Exponent
0.0
0.5
1.0
1.5
2.0
0.3
0.4
0.5
0.6
0.7
0.8
fraction of day

Figure 4

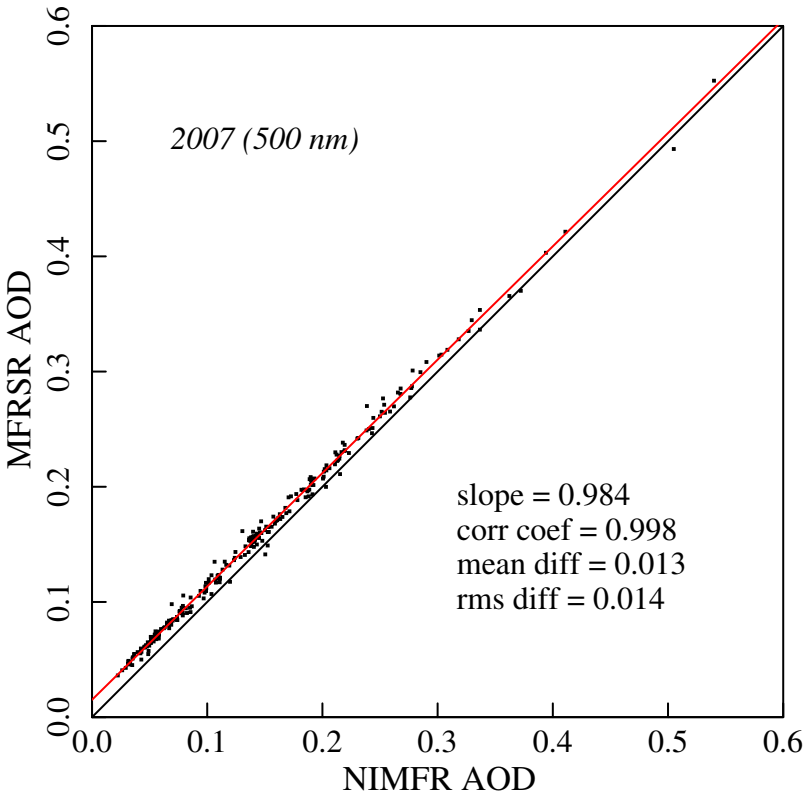
2007 (500 nm)
slope = 0.984
corr coef = 0.998
mean diff = 0.013
rms diff = 0.014
MFRSR AOD
NIMFR AOD
0.0
0.1
0.2
0.3
0.4
0.5
0.6

Figure 5

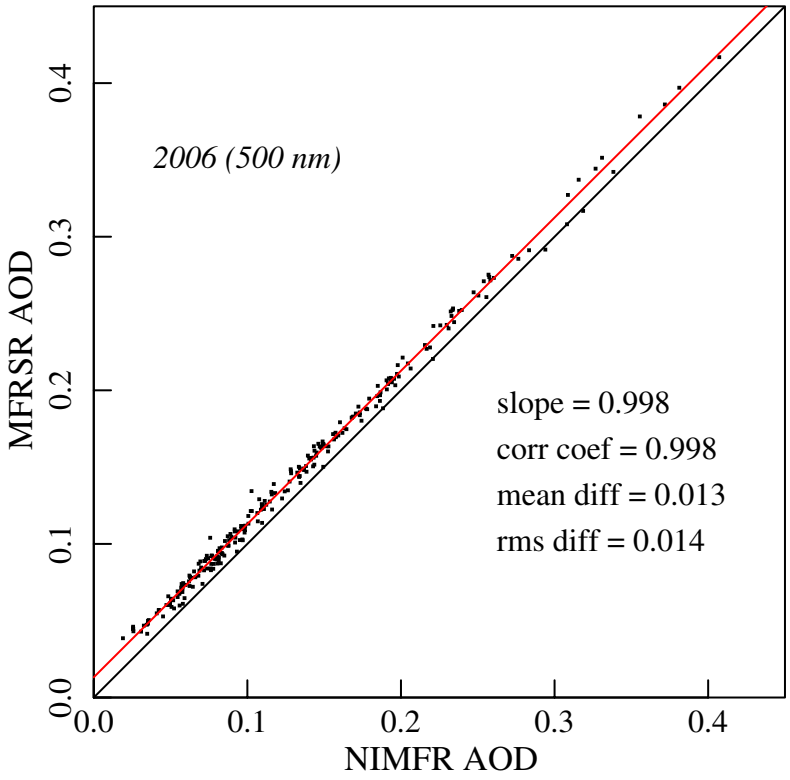
2006 (500 nm)
slope = 0.998
corr coef = 0.998
mean diff = 0.013
rms diff = 0.014
MFRSR AOD
NIMFR AOD
0.0
0.1
0.2
0.3
0.4

Figure 6

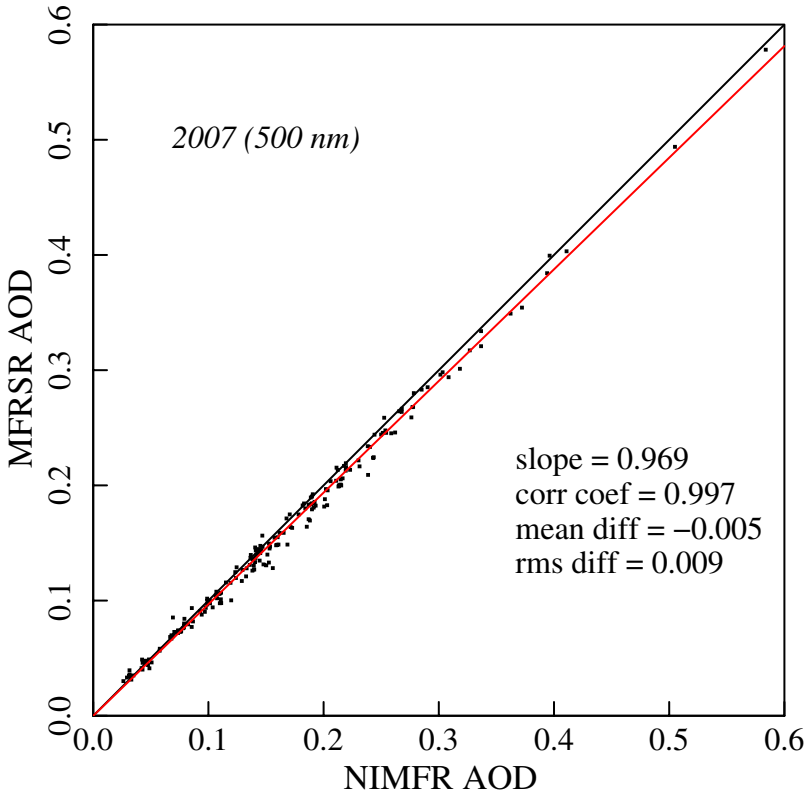
2007 (500 nm)
slope = 0.969
corr coef = 0.997
mean diff = –0.005
rms diff = 0.009
MFRSR AOD
NIMFR AOD
0.0
0.1
0.2
0.3
0.4
0.5
0.6

Figure 7

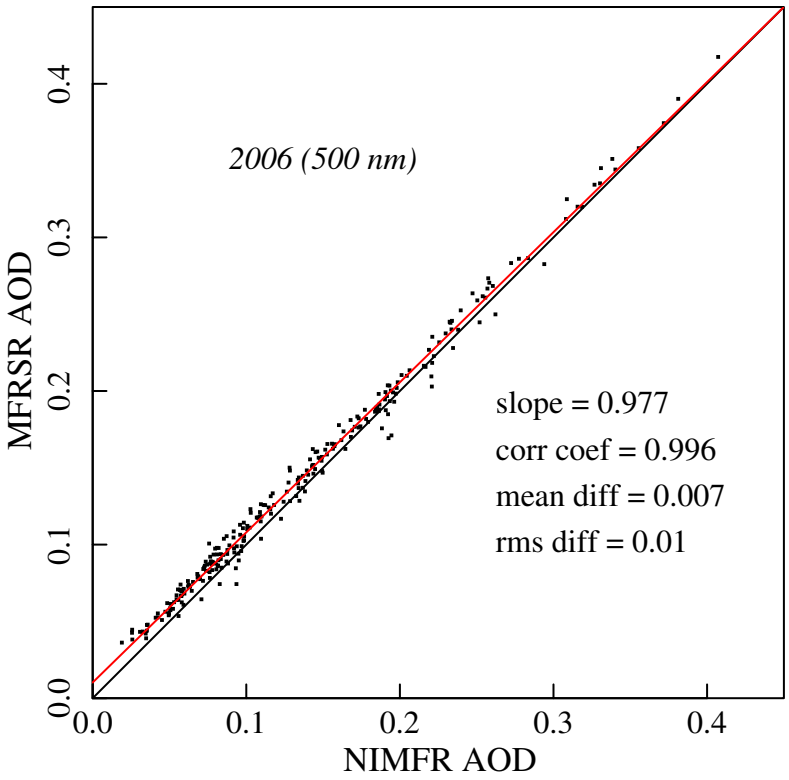
2006 (500 nm)
slope = 0.977
corr coef = 0.996
mean diff = 0.007
rms diff = 0.01
MFRSR AOD
NIMFR AOD
0.0
0.1
0.2
0.3
0.4

Figure 8

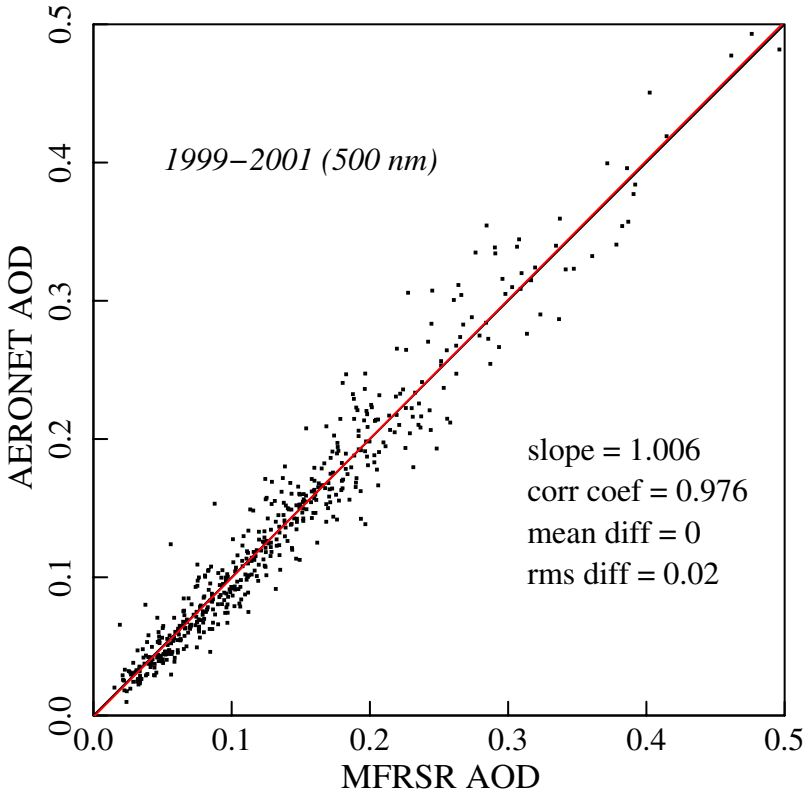
1999–2001 (500 nm)
slope = 1.006
corr coef = 0.976
mean diff = 0
rms diff = 0.02
AERONET AOD
MFRSR AOD
0.0
0.1
0.2
0.3
0.4
0.5

Figure 9

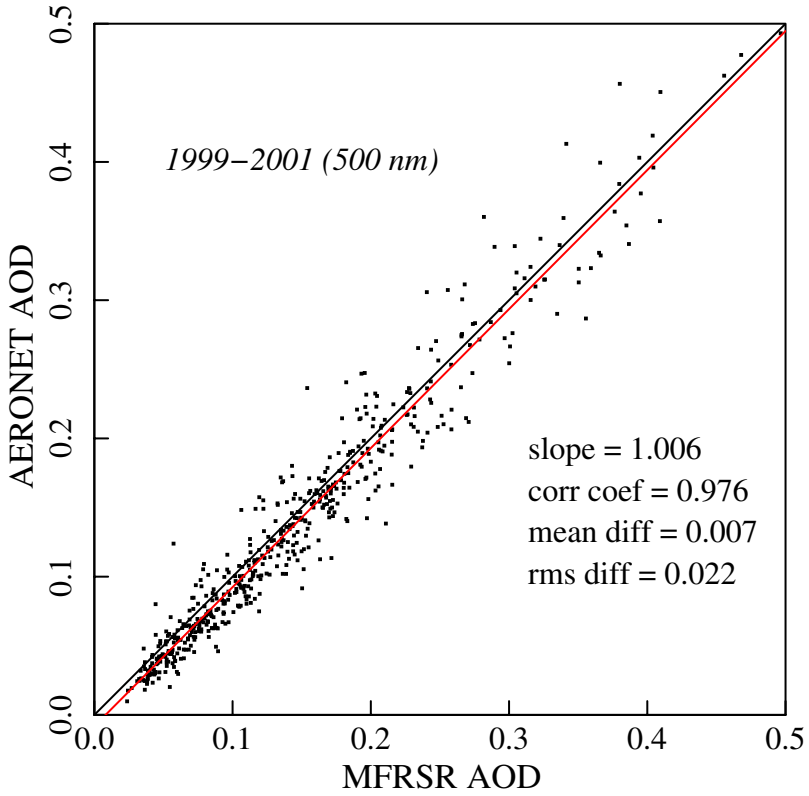
1999–2001 (500 nm)
slope = 1.006
corr coef = 0.976
mean diff = 0.007
rms diff = 0.022
AERONET AOD
MFRSR AOD
0.0
0.1
0.2
0.3
0.4
0.5

Figure 10

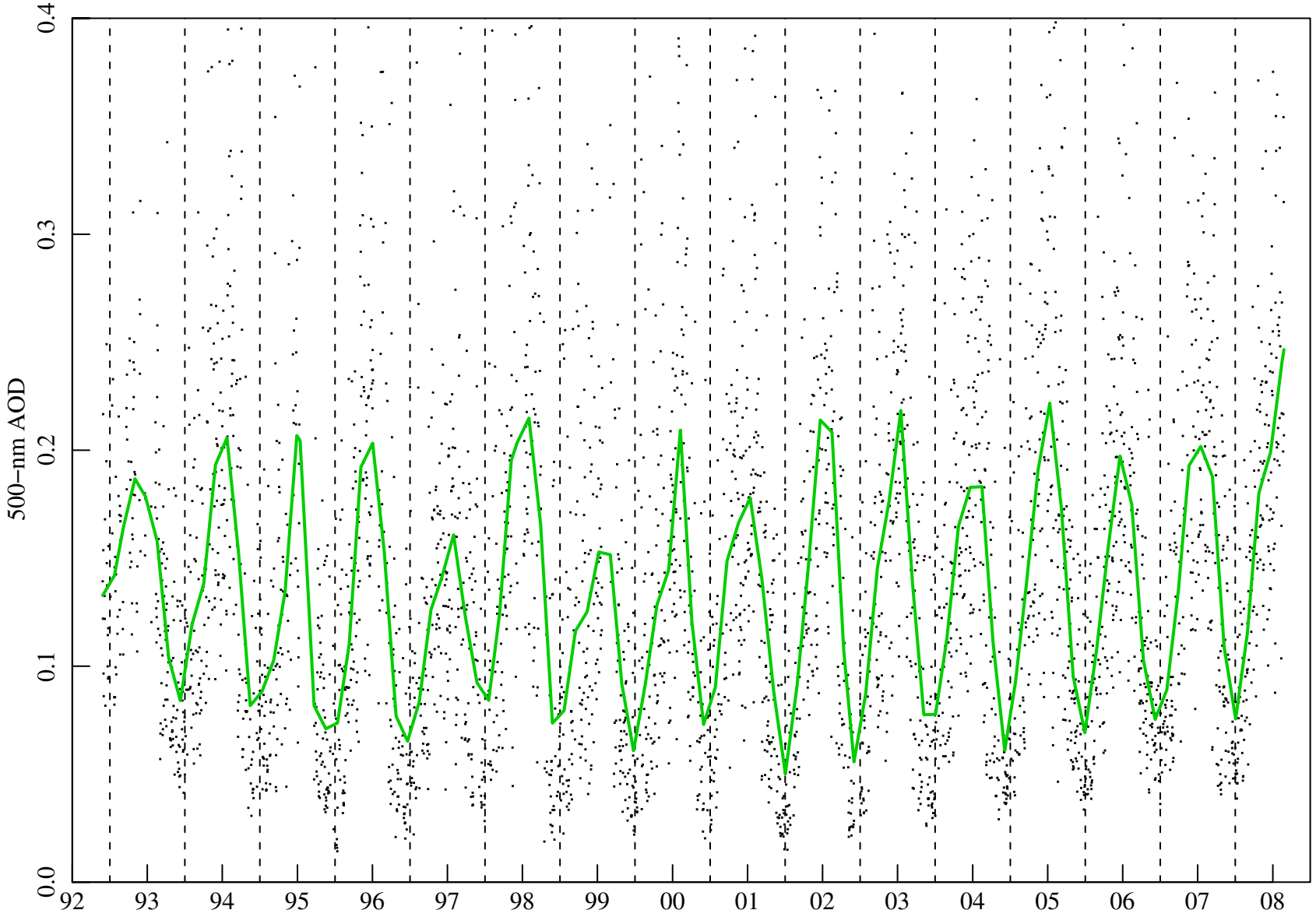
500−nm AOD
0.0
0.1
0.2
0.3
0.4
92
93
94
95
96
97
98
99
00
01
02
03
04
05
06
07
08

Figure 11

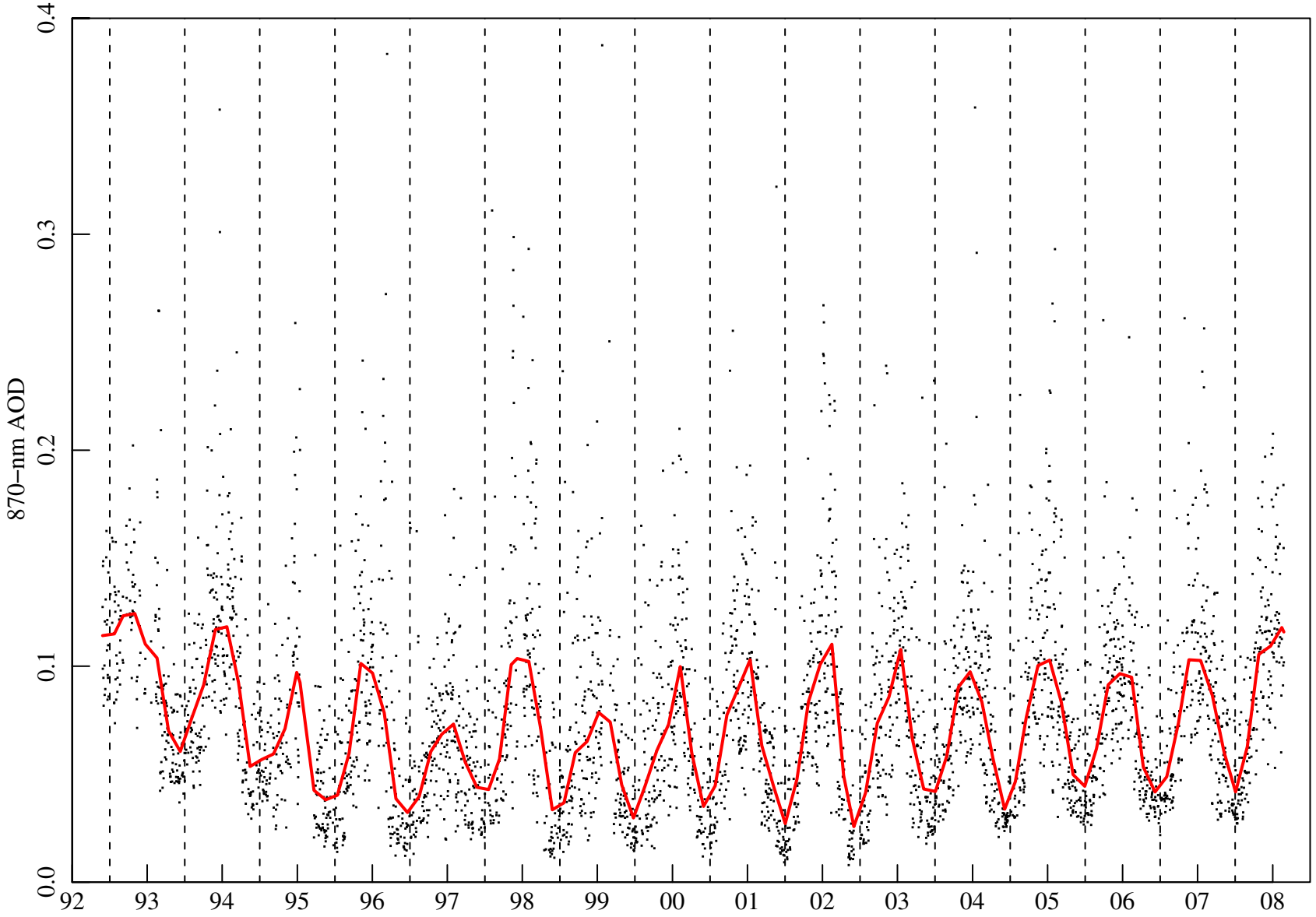
870−nm AOD
0.0
0.1
0.2
0.3
0.4
92
93
94
95
96
97
98
99
00
01
02
03
04
05
06
07
08

Figure 12

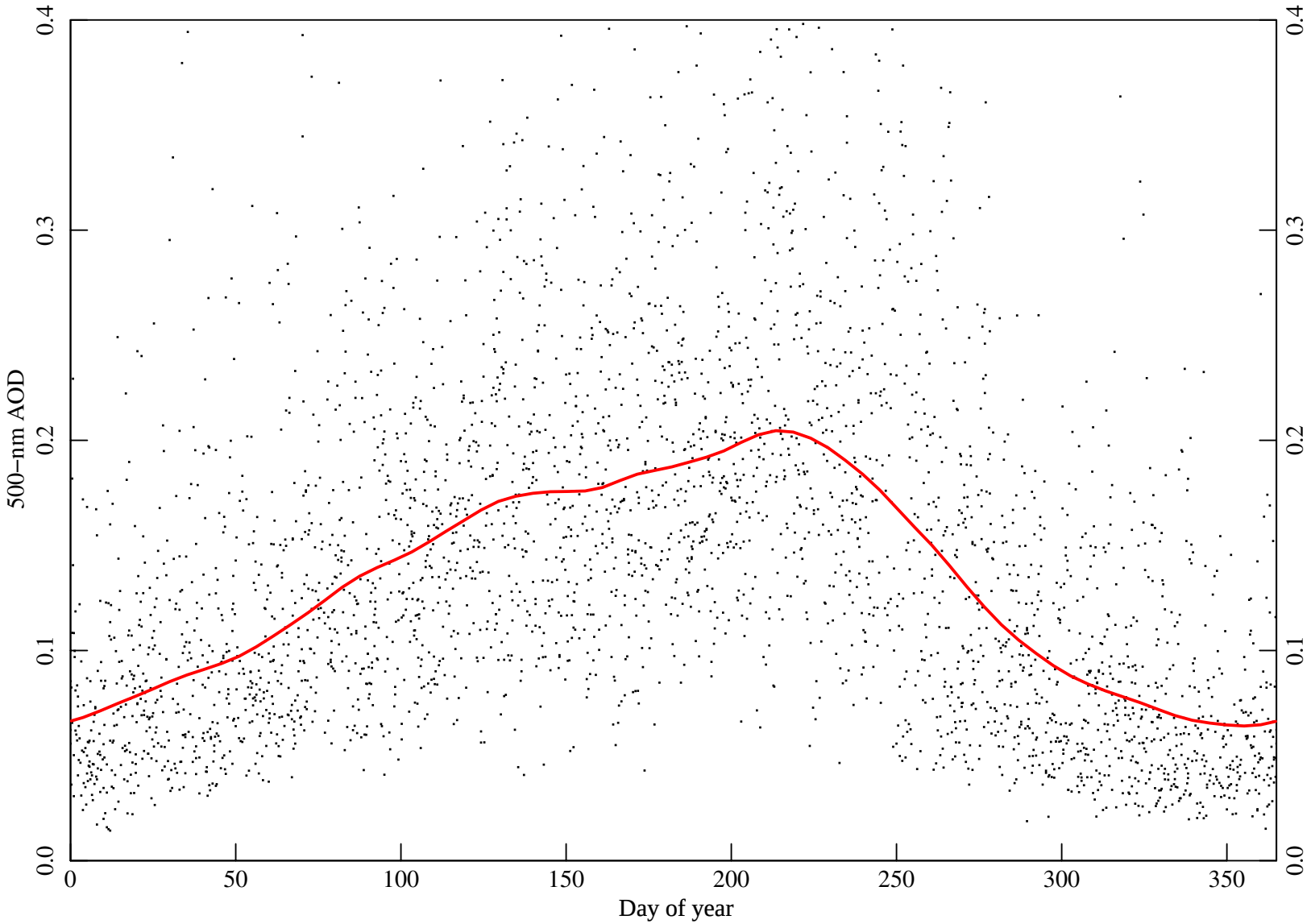

Figure 13

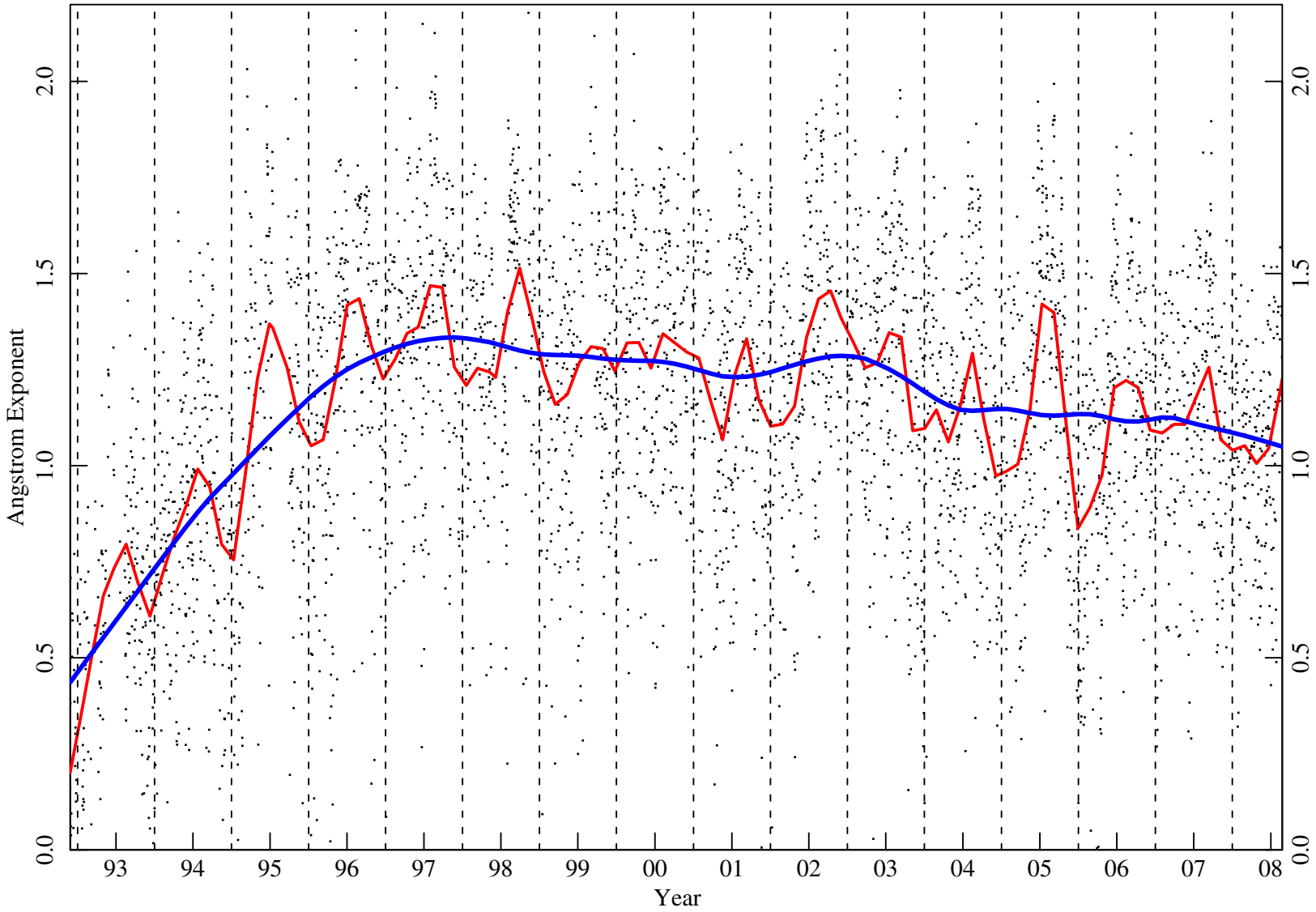
Angstrom Exponent
0.0
0.5
1.0
1.5
2.0
93
94
95
96
97
98
99
00
01
02
03
04
05
06
07
08
Year

Figure 14

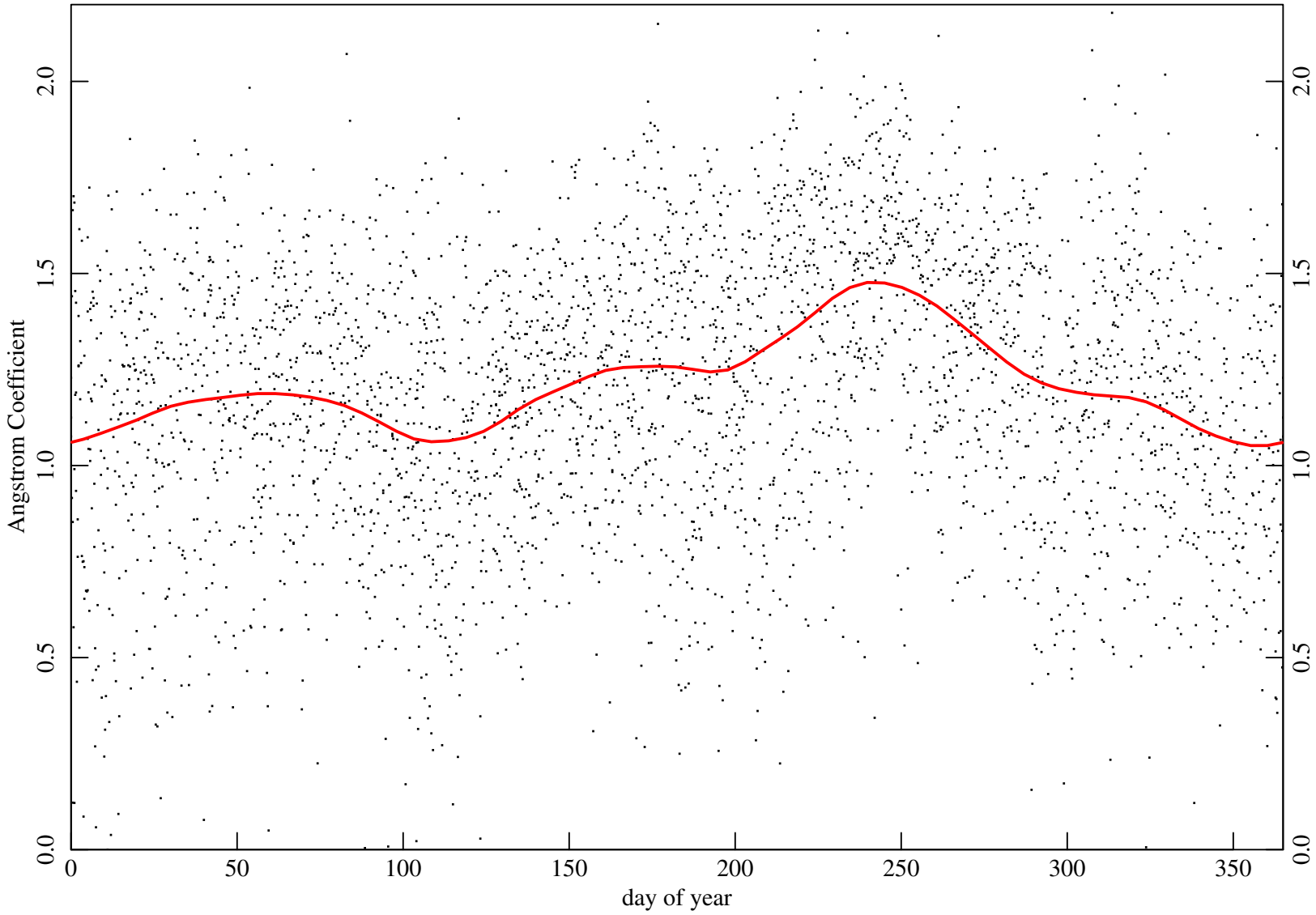
Angstrom Coefficient
0.0
0.5
1.0
1.5
2.0
0
50
100
150
200
250
300
350
day of year

Figure 15

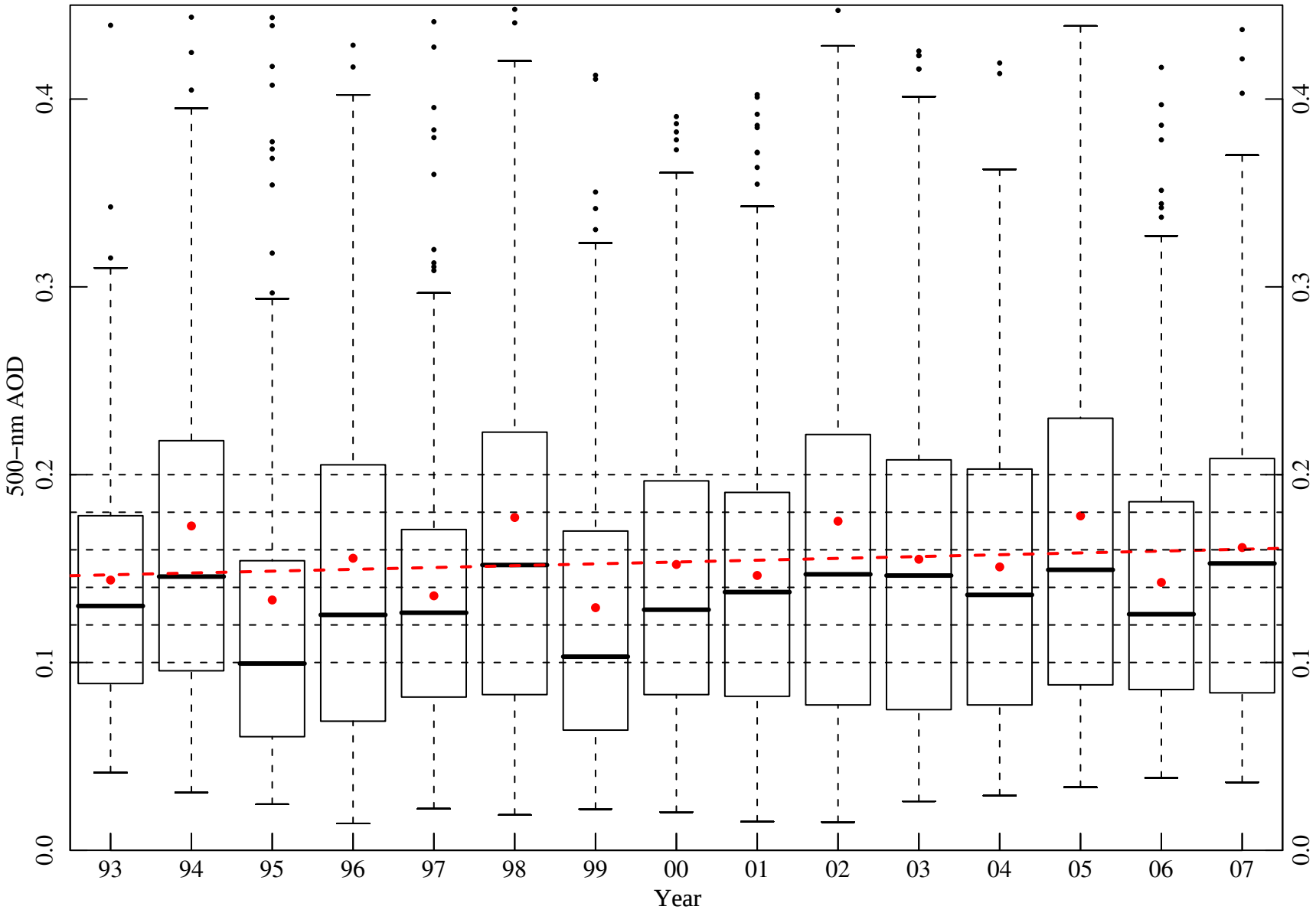
500−nm AOD
0.0
0.1
0.2
0.3
0.4
93
94
95
96
97
98
99
00
01
02
03
04
05
06
07
Year

Figure 16

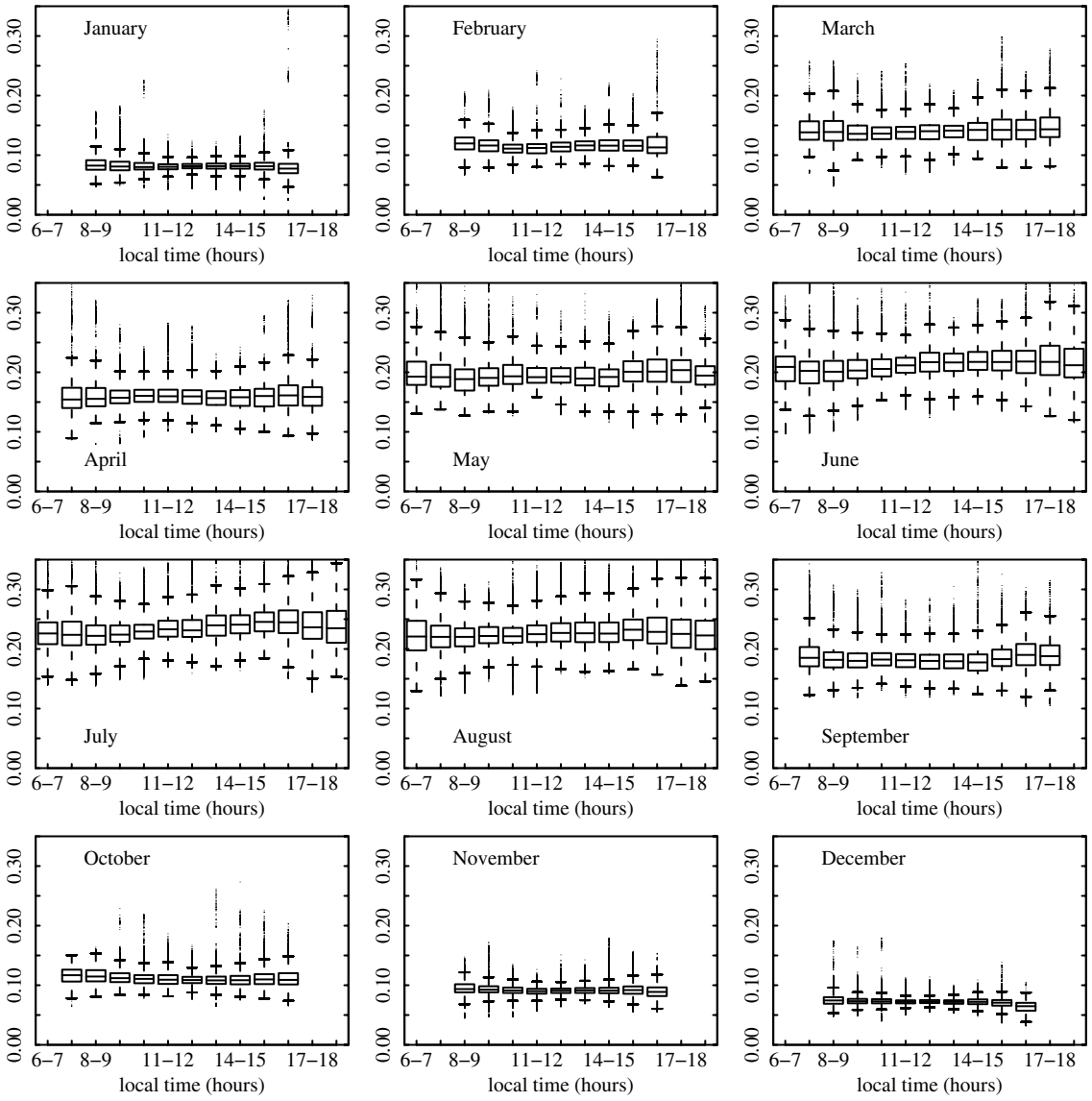
January
February
March
April
May
June
July
August
September
October
November
December
0.00
0.10
0.20
0.30
6–7
8–9
11–12
14–15
17–18
local time (hours)

Figure 17

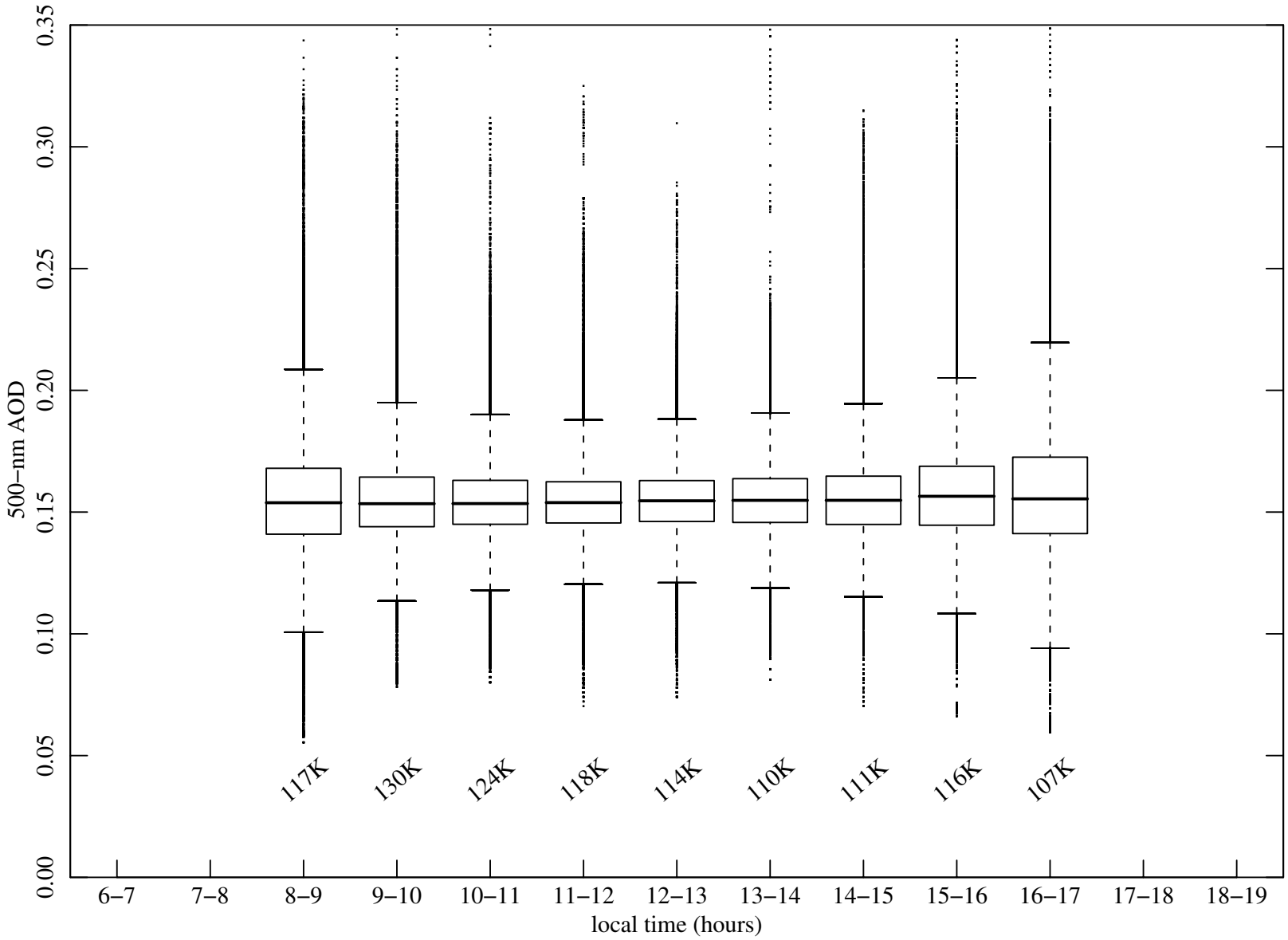
500−nm AOD
0.00
0.05
0.10
0.15
0.20
0.25
0.30
0.35
117K
130K
124K
118K
114K
110K
111K
116K
107K
6−7
7−8
8−9
9−10
10−11
11−12
12−13
13−14
14−15
15−16
16−17
17−18
18−19
local time (hours)

Figure 18